Magnetic coupling at the interface between ultrathin tetragonal CuO and La$_{0.7}$Sr$_{0.3}$MnO$_3$

Digbijaya Palai [1,2,*] Ravinder Kumar [1,2,3,*] M. Tahir [4] P. Gupta [5] S. N. Sarangi,[1,2] S. Bedanta,[5]
G. Tripathy,[1,2] S. Mukhopadhyay,[4] Z. Hossain,[4] and D. Samal [1,2,†]

[1]*Institute of Physics, Bhubaneswar 751005, India*
[2]*Homi Bhabha National Institute, Anushaktinagar, Mumbai 400094, India*
[3]*Department of Physics, Morgan State University, Baltimore, Maryland 21251, USA*
[4]*Department of Physics, Indian Institute of Technology, Kanpur 208016, India*
[5]*Laboratory for Nanomagnetism and Magnetic Materials (LNMM), School of Physical Sciences, National Institute of Science
Education and Research (NISER), an OCC of Homi Bhabha National Institute (HBNI), Jatni 752050, Odisha, India*

High-symmetry rocksalt type tetragonal CuO (T-CuO) does not exist in bulk but can be synthesized via thin film epitaxy limited to a few unit cells (3, 4) thick and above which it relaxes to its bulk tenorite structure. Direct probe into magnetic properties of T-CuO layer has been a challenge because of its ultrathin limit. Here, we demonstrate the interfacial magnetic coupling between ultrathin T-CuO and ferromagnetic (La$_{0.7}$Sr$_{0.3}$MnO$_3$) layers in an epitaxial CuO/La$_{0.7}$Sr$_{0.3}$MnO$_3$ bilayer grown on (001)-oriented SrTiO$_3$. We observe a positive exchange bias shift of ~30 Oe at 2 K in CuO/La$_{0.7}$Sr$_{0.3}$MnO$_3$ bilayer. The observation of positive exchange bias indicates that there exists antiferromagnetic exchange coupling between Mn and Cu moments at the interface. Notably, the exchange bias vanishes at 5 K and it is discussed in view of the proposed spin structure revealed from low-energy muon spin rotation and x-ray magnetic circular dichroism study [Phys. Rev. B **103**, 224429 (2021)]. Furthermore, an enhanced Gilbert damping, linewidth broadening and larger inhomogeneous $4\pi M_{\mathrm{eff}}$ value from in-plane ferromagnetic resonance measurements, are the direct consequence of antiferromagnetic exchange coupling at the CuO/La$_{0.7}$Sr$_{0.3}$MnO$_3$ interface. Combining both static and dynamic magnetic characterization, we establish an understanding of interfacial exchange coupling in CuO/La$_{0.7}$Sr$_{0.3}$MnO$_3$ bilayer.

I. INTRODUCTION

After the discovery of high-T_C superconductivity (HTSC) in the Ba-La-Cu-O system in 1986, a large family of copper oxide systems have been studied extensively to understand the effect of doping, crystal structure and dimensionality on their electronic properties [1]. The evolution of superconducting state upon doping quasi two-dimensional (2D) insulating (Mott insulators) cuprates indicate that electron correlations in 2D CuO$_2$ planes play a crucial role for this class of materials [2,3]. Archetype binary cupric oxide (CuO) that exhibits correlation induced insulating ground state lacks the requisite crystal chemistry (2D CuO$_2$ plaquettes separated by charge reservoir layers) for realizing superconductivity and is fundamentally different from that of copper oxide based superconducting materials. It crystallizes in a low-symmetry $C2/c$ monoclinic structure (tenorite) [4] and its magnetic behavior is dominated by quasi-one-dimensional (1D) antiferromagnetic (AFM) chains [5–9]. Unlike other members (MnO, FeO, CoO, and NiO) in the monoxide series that crystalize in the cubic rocksalt structure with small lattice distortion ($< 2\%$) at low temperature [10–13] and exhibit an increasing trend of the Néel temperature (T_N) with increasing

atomic number (MnO: $T_N = 118$ K, FeO: $T_N = 200$ K, CoO: $T_N = 291$ K, and NiO: $T_N = 523$ K), the monoclinic CuO shows a substantial departure from this trend by having a relatively lower T_N (~230 K) [8,14]. This is caused by the complex interplay of lattice structure (Cu–O–Cu bond angle, $\phi = 146°$), chemical bonding, and the underlying exchange coupling.

Despite the fact that bulk CuO does not crystallize in cubic or tetragonal phase, thin film epitaxy has rather been proven to be successful in stabilizing a high symmetric tetragonal form of CuO ($c/a \sim 1.34$) on a SrTiO$_3$ (001) substrate up to a thickness of few unit cells by controlling the rigidity of the oxygen sublattice [15–17]. The epitaxy renders a platform to arrest cooperative Jahn-Teller distortion in CuO, resulting in a more symmetric structure. Tetragonal CuO (T-CuO) has attracted attention because of its structural similarity to the cuprates as a 3D counterpart where the CuO planes are electronically interconnected by Cu d_{xz}, d_{yz}, d_{z^2} and O p_z orbitals. Its structure consists of 2D CuO planes (stacked along c-axis) made out of edge-sharing CuO$_4$ plaquettes and each CuO plane can be regarded equivalent to two interpenetrating CuO$_2$ sublattices [Fig. 1(d)]. There exists a subtle structural difference between CuO$_2$ plane in HTSC and the CuO plane in T-CuO (while CuO$_4$ plaquettes in case of T-CuO coordinate in an edge shared geometry [Fig. 1(c)], the same in CuO$_2$ plane form corner shared network [Fig. 1(d)]) [17]. Effective one-band model based on Zhang-Rice singlets (ZRS) have
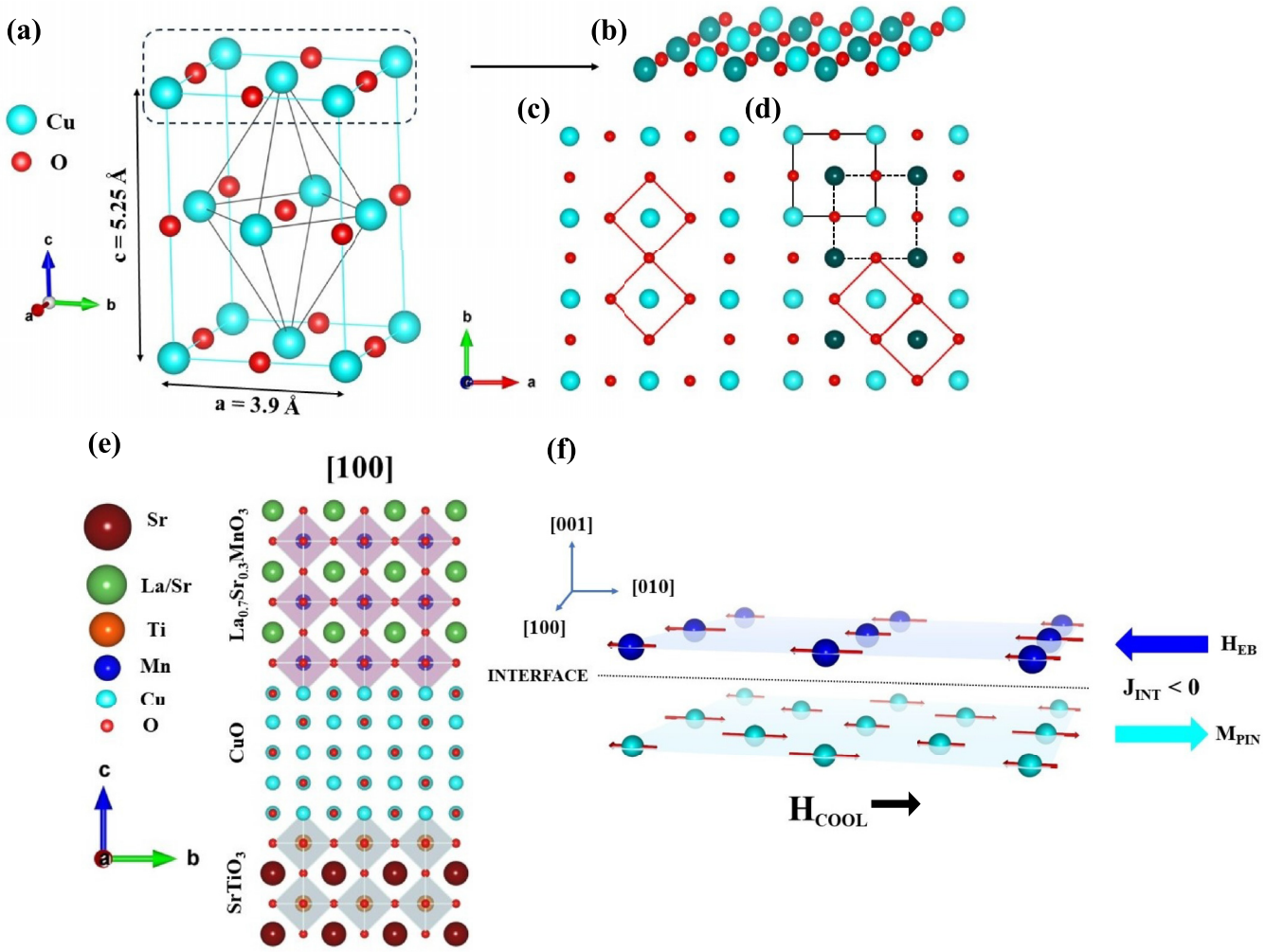
FIG. 1. (a) The tetragonal crystal structure of CuO. (b) Slab of T-CuO viewed along [001] face. Bright and dark cyan atoms represent two different sublattices. (c) CuO_2 plane consisting of corner shared CuO_4 plaquettes. (d) Each CuO plane can be viewed to consists of two interpenetrating CuO_2 sublattices (The solid and dotted black squares belong to two different sublattices). The red squares represent edge shared CuO_4 plaquettes spanning the T-CuO plane. (e) Sketch of CuO/LSMO bilayer grown on STO substrate viewed along [100] direction. (f) Schematic interfacial spin configuration giving rise to a positive exchange bias effect in the T-CuO/LSMO bilayer. The cooling field (H_{COOL}) induces a net magnetization M_{PIN}(denoted by the cyan-colored arrow) in the T-CuO layer (larger and smaller arrows denote spins along and opposite to H_{COOL}) in the direction of H_{COOL}, which is pinned due to defects. Due to the AFM coupling ($J_{INT} < 0$) at the interface, M_{PIN} induces an effective positive exchange bias (H_{EB}, denoted by the blue-colored arrow) for the ferromagnetic LSMO layer, in the direction opposite to H_{COOL}.

been invoked to describe the low-energy electronic excitations of T-CuO [17,18]. The study based on scanning tunneling spectroscopy measurement on ultrathin T-CuO films finds it to have a charge transfer gap of 3.68 eV [19].

Density functional theory (DFT) calculations have suggested that T-CuO will have a very high antiferromagnetic (AFM) ordering temperature close to $T_N = 800$ K [20,21]. However, direct measurement of magnetic properties on T-CuO thin films using the conventional magnetometry technique has been hindered due to its ultrathin limit. Nevertheless, there have been experimental attempts to delve into the magnetic structure of ultrathin T-CuO layer by resonant inelastic x-ray scattering (RIXS) [22], low-energy muon spin rotation (LE-μSR) and x-ray magnetic circular dichroism (XMCD) investigations [23]. RIXS performed on T-CuO thin films at 20 K revealed dispersing spin wave excitations on

two cuprate like AFM sublattices indicating the presence of AFM correlation [22]. The recent study involving muon spin polarization decay on T-CuO thin films indicated an AFM order with a transition temperature about 200 K. More particularly from XMCD, it was found that there exists pinned Cu^{2+} magnetic moments along the in-plane direction close to the surface of the T-CuO film and this pinning is primarily caused by an AFM ordering of underlying spins moments. Remarkably, the pinning was found to be robust below 3 K and as the temperature increased the pinned moments start to rotate along the direction of field and become reversible.

Apart from the highly sensitive scattering and spectroscopic measurements used to delve into magnetic structure in ultrathin films, the phenomenon of magnetic exchange bias (EB) effect has been employed as a powerful method to probe the magnetism in thin films. EB effect refers to the

unidirectional shift of M(H) loop along the magnetic field axis in a coupled FM/AFM bilayer system [24,25]. Zhou *et al.* used this method to directly demonstrate the antiferromagnetic ground state of one mono layer FeSe film grown on SrTiO$_3$ substrate [26]. In this report, we present the direct observation of low temperature (below 5 K) positive exchange bias (PEB) effect in a CuO ($\sim$1 nm)/La$_{0.7}$Sr$_{0.3}$MnO$_3$ ($\sim$10 nm) bilayer (La$_{0.7}$Sr$_{0.3}$MnO$_3$ (LSMO) is a well-known conducting ferromagnetic (FM) system above room temperature) indicating the presence of antiferromagnetic correlation in ultrathin T-CuO layer. The observation of PEB indicates there exists AFM type exchange coupling between Mn and Cu moments at the CuO/La$_{0.7}$Sr$_{0.3}$MnO$_3$ interface [27,28]. To further shed light on the role of interfacial exchange coupling at CuO/LSMO interface, we have performed ferromagnetic resonance (FMR) measurement at 300 K on CuO/LSMO and LSMO thin films. The significant increase (3-fold) in the relaxation mechanism characterized by the Gilbert damping parameter, FMR linewidth broadening and a large inhomogeneous $4\pi M_{\text{eff}}$ in the CuO/LSMO bilayer in comparison with bare LSMO (10 nm) layer, suggests the possibility of interfacial antiferromagnetic exchange coupling. Our study deepens the understanding of the interfacial exchange coupling in CuO/LSMO bilayer by integrating both static and dynamic magnetic characterizations.

II. EXPERIMENT

Thin films of CuO ($\sim$1 nm)/LSMO($\sim$ 10 nm) bilayer as well as LSMO (10 and 20 nm) were deposited on STO (001) substrates by reflection high energy electron diffraction (RHEED) assisted pulsed laser deposition (KrF excimer laser with $\lambda = 248$ nm) at a repetition rate of 1 Hz, and a laser fluence of 1.6 J/cm^2. Polycrystalline LSMO and CuO ceramic targets prepared by solid state reaction method were used for the growth of respective layers. The most homogeneous part of the laser beam was selected using a rectangular mask (15$\times$4 mm^2) and an image of the mask was created on the stoichiometric targets with a lens. Before deposition the target was preablated for 2 minutes. Thin films were grown at a substrate temperature of 650 °C and in the presence of 0.2 mbar of O$_2$ pressure. After growth, these films were cooled down to room temperature at a rate of 10 °C/min in an O$_2$ atmosphere (0.2 mbar) to eliminate any oxygen deficiency. *In situ* RHEED was used to monitor the growth and examine the formation of rocksalt like structure of CuO in ultrathin limit. Structural characterization was performed by x-ray diffraction using Cu K$_{\alpha 1}$ source ($\lambda = 1.54059$ Å). The thicknesses of the thin films were estimated from x-ray reflectivity (XRR) measurements using PAnalytical X'pert PRO four circle diffractometers. Magnetic measurements of all samples were performed using a superconducting quantum interference device (SQUID) magnetometer in the temperature range of 2 to 370 K. The ferromagnetic resonance (FMR) measurements were carried out using the Quantum Design NanOsc Phase FMR setup.

III. RESULTS AND DISCUSSION

A. Structural characterization

Figure 2 summarizes the structural analysis of LSMO, and CuO/LSMO bilayer thin films grown on STO (001) substrate.
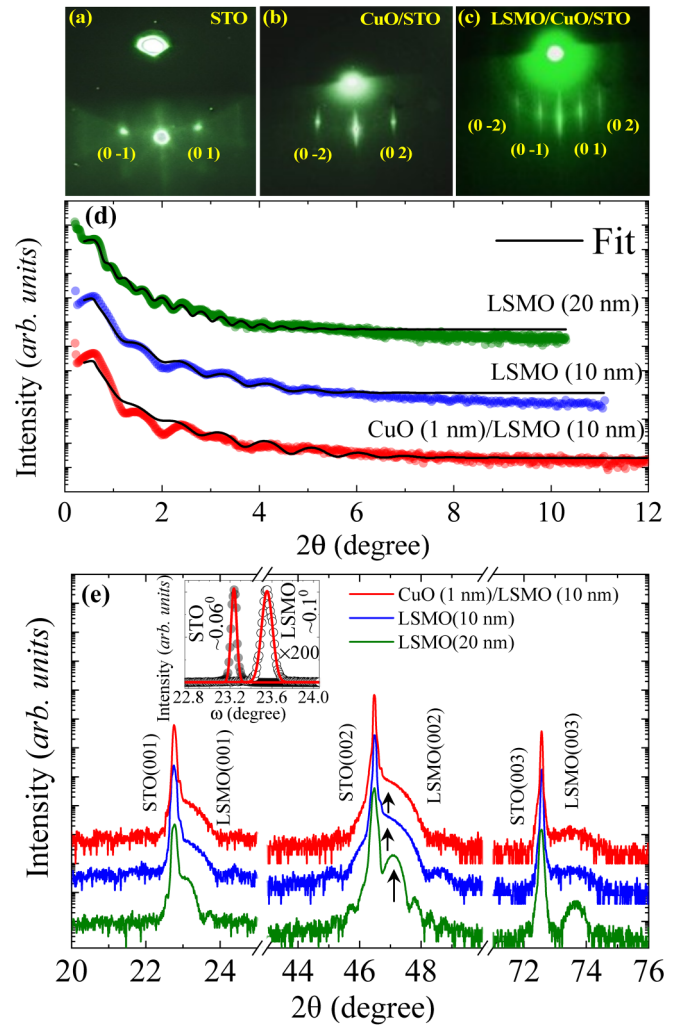

FIG. 2. Structural characterization by using RHEED and XRD techniques. RHEED pattern of (a) STO (001) at 650 °C, (b) after the growth of ultrathin T-CuO layer at 650 °C and (c) CuO/LSMO bilayer after the growth of LSMO on top of T-CuO layer at 650 °C. (d) XRR data of bare LSMO (10 nm) and CuO (1 nm)/LSMO(10 nm) bilayer samples. (e) XRD $\theta - 2\theta$ patterns of bare LSMO and CuO/LSMO bilayer samples. Inset: The FWHMs of the ω scan performed around (002) plane for LSMO (20 nm) film and STO substrate.

To ensure the growth of rocksalt type T-CuO on STO (001), we monitored the real-time evolution of RHEED spectra. Based on crystal symmetry, the allowed diffraction peaks for a rocksalt structure ($Fm\bar{3}m$ space group) in two dimensions (2D) are characterized by the reflection condition, $h + k = 2n$, i.e., (h, k) indices are unmixed [29]. In Figs. 2(a)–2(c), we show the RHEED diffraction patterns measured along (0 1) direction of STO (001) during the growth of T-CuO as well as LSMO films. During the growth of T-CuO film, we observed streaky RHEED pattern [Fig. 2(b)] along (0 −2) and (0 2) direction indicating the 2D growth of T-CuO on STO. However, we did not observe any RHEED spot along (0 −1) and (0 1) directions. The absence of (0 −1) and (0 1) reflections (mixed *h, k*) is in agreement with the exclusion principle of reflection for a rocksalt-type structure [15,29].

Further, during the growth of perovskite LSMO on T-CuO, we strikingly observe the reappearance of (0 −1) and (0 1) reflections [Fig. 2(c)] along with the (0 −2) and (0 2) reflections. This is expected since all combinations of (*h, k*) reflections are allowed for a cubic perovskite structure [29]. In essence, the reappearance of (0 1) diffraction spots in between (0 2) ones in Fig. 2(c) captures a clear change in crystal symmetry and demonstrates the successful growth of a perovskite LSMO layer on a rocksalt type T-CuO. X-ray reflectivity (XRR) measurements were carried out to estimate the thicknesses of individual layers and the corresponding results are shown in Fig. 2(d). By fitting the XRR experimental data, the thickness of different films is estimated to be LSMO (∼10 nm), CuO (∼1 nm)/LSMO (∼10 nm), and LSMO (∼20 nm). The observation of Kiessig fringes shown in Fig. 2(d) suggest smooth and sharp interfaces. The $\theta - 2\theta$ XRD pattern in Fig. 2(e) reveals the characteristic (00*l*) Bragg's reflections indicating *c*-axis oriented growth of LSMO layer. No additional reflections were observed for any of the samples, confirming the absence of any parasitic phase. The observation of trails of Lau thickness interference fringes around the (002) peak of LSMO (∼20 nm) film denotes coherent and homogenous growth of the film. Additionally, the very low value ∼0.1° of the full width at half maximum (FWHM) obtained from ω scan [see inset of Fig. 2(e)] indicates a very good crystallinity of LSMO (∼20 nm) film. Since the T-CuO film was too thin (∼1 nm), we could not observe any distinct diffraction peak associated with T-CuO layer. The *c*-axis lattice parameter of LSMO (∼20 nm) estimated from (002) diffraction peak position is found to be 3.862 Å, a decreased value as compared to the bulk LSMO sample ($a_{pc} \sim 3.889$ Å) [30]. By considering an idealistic fully in-plane strained case with $a = b = 3.905$ Å (lattice parameter of STO) and considering the unit-cell volume conservation, one would expect the *c*-axis lattice parameter of LSMO (∼20 nm) to be ∼3.857 Å. The observed shortened *c*-axis lattice parameter indicates that the LSMO (∼20 nm) film experiences an in plane tensile strain from the underlying STO substrate. In case of LSMO (∼10 nm) and CuO (∼1 nm)/LSMO (∼10 nm) bilayer, we observed a broad shoulder around the (002) of STO corresponding to (002) LSMO reflection as shown in Fig. 2(e). The broadening of peaks in LSMO (∼10 nm) and CuO (∼1 nm)/LSMO (∼10 nm) is related to the finite film thickness effect where the in-plane lattice parameters of the film match close to that of STO substrate [31,32]. In essence the detailed structural investigation confirms the successful growth of LSMO and T-CuO/LSMO bilayer thin films. Hereafter, the CuO (∼1 nm)/LSMO (∼10 nm) is abbreviated as CuO/LSMO for the sake of brevity.

B. Magnetism

Figures 3(a) and 3(b) show the temperature-dependent magnetization under zero field cooled (ZFC) and field cooled (FC) mode at an applied external magnetic field (in-plane) of 100 Oe for LSMO (10 nm) and CuO/LSMO films, respectively. The ferromagnetic transition temperature (T_C) determined from the first derivative of the ZFC curve is found to be ∼315 K for both of the above films, which is in good agreement with the previously reported LSMO/STO
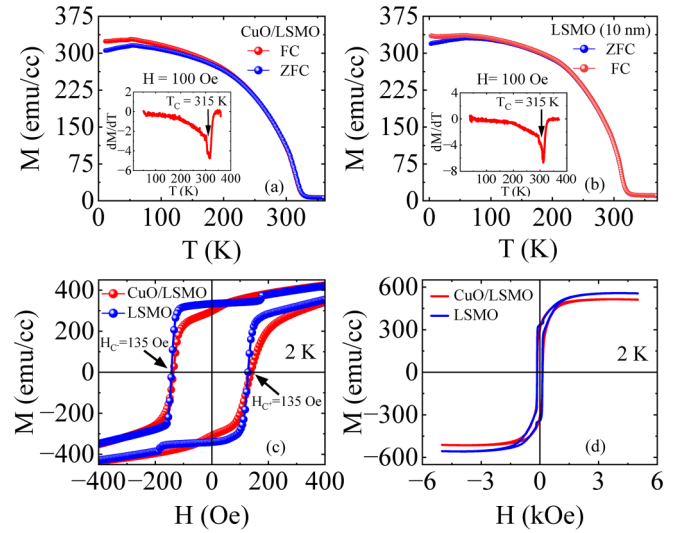

FIG. 3. [(a) and (b)] Temperature dependence of magnetization of bare LSMO (10 nm) layer and CuO/LSMO bilayer under an in-plane magnetic field of 100 Oe. (Insets) T_C is determined by dM/dT of the ZFC curve. (c) Enlarged plot of $M(H)$ loop of bare LSMO (10 nm) layer and CuO/LSMO bilayer at 2 K in ZFC mode. (d) $M(H)$ loop of bare LSMO (10 nm) layer and CuO/LSMO bilayer at 2 K in ZFC mode.

epitaxial thin films with having thickness in the same range [33]. The lowering of T_C as compared to the LSMO bulk value (∼370 K) could be related to finite size and strain induced effects [33–37]. Since the T_C in case of bare LSMO (10 nm) film and CuO/LSMO bilayer are found to be identical, it indicates that underlayer T-CuO has no detrimental effect on the magnetic properties of LSMO. Figures 3(c) and 3(d) show in plane ZFC M(H) plot at 2 K for CuO/LSMO bilayer and bare LSMO (10 nm) thin films. Both films show symmetrical hysteresis loops of coercive fields $H_C \approx 135$ Oe [Fig. 3(c)], but different saturation magnetization ($M_S = 557$ emu/cc and 514 emu/cc for the bare LSMO (10 nm) and CuO/LSMO samples, respectively) [Fig. 3(d)]. The observed decrease in saturation magnetization in the CuO/LSMO bilayer structure suggests the possible occurrence of antiferromagnetic interfacial coupling at the interface between the T-CuO and LSMO layers. The observation of magnetization jump around 173 Oe in the M(H) loop of bare LSMO (10 nm) film at 2 K could be related to the Barkhausen jump [Fig. 3(c)] [38]. These jumps are generally caused by the irreversible motion of the domain walls between the two regions of opposite magnetizing forces, as reported in various oxide thin films [39,40].

We now examine the possibility of realizing the interfacial FM/AFM coupling effect at the interface between LSMO and T-CuO layers by investigating magnetic exchange bias effect. Typically, a bilayer consisting of a FM and an AFM (with the Curie temperature (T_C) of FM greater than the Néel temperature (T_N) of AFM) when cooled in a static magnetic field across the T_N, a unidirectional exchange anisotropy field gets locked in and gives rise to the EB effect [41,42]. The exchange bias field H_{EB} and the coercive field H_C are given as $|H_{C-} - H_{C+}|/2$ and $|H_{C-} + H_{C+}|/2$, where H_{C-} and H_{C+} are the coercive fields at which the magnetization reaches zero
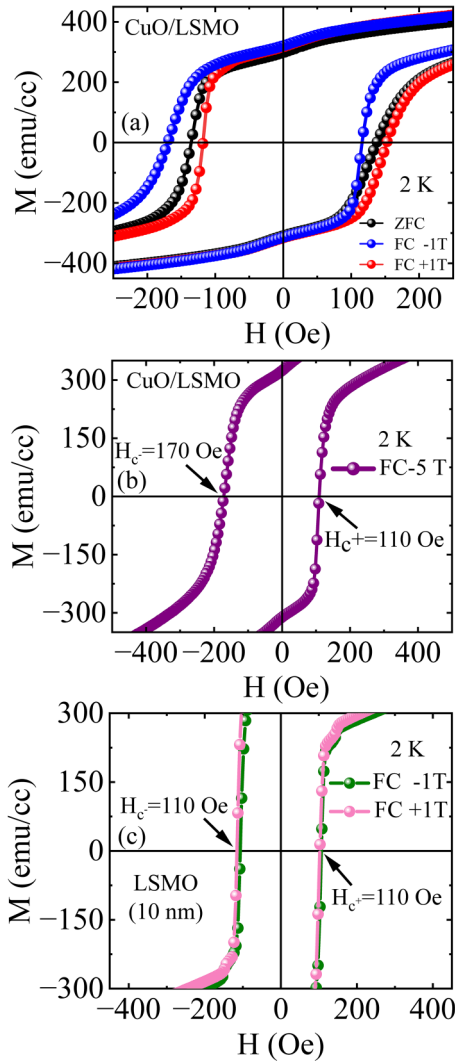
FIG. 4. Exchange bias measurements. Shifted $M(H)$ loops of CuO/LSMO bilayer measured at 2 K after the sample is cooled down (a) under FC mode of $+1$ and -1 T, (b) under FC mode of -5 T, and (c) enlarged $M(H)$ symmetrical loop of single LSMO (10 nm) layer under cooling field of -1 and $+1$ T.

during the tracing of the negative and positive branches of the hysteresis loop, respectively. Figure 4(a) shows the in-plane $M(H)$ loops measured at 2 K in FC mode from 370 K in applied fields of $+1$ and -1 T. It is seen that $M(H)$ loops shift along the direction of cooling fields which are referred to as positive exchange bias. For the sake of comparison, we have also shown the symmetrical ZFC $M(H)$ loop [Fig. 4(a)] measured at 2 K for CuO/LSMO bilayer. The magnitudes of the exchange bias field H_{EB} at 2 K are found to be 27 ± 2.4 and 17 ± 2.3 Oe for the cooling fields of -1 T and $+1$ T, respectively. However, no EB effect is observed in the case of bare LSMO (10 nm) layer [Fig. 4(c)] after field cooling it from 370 K in an applied field of -1 and $+1$ T. The observed EB effect is considered to be the direct manifestation of the interfacial exchange coupling between LSMO and ultrathin T-CuO thin films. Since a comparatively larger H_{EB} (27 ± 2.4 Oe) arises in the negative FC mode, we examined the evolution of EB effect under different negative cooling fields at

2 K, which shows a maximum value of $H_{EB} = 30 \pm 2.9$ Oe [Fig. 4(b)] at a cooling field of -5 T.

Figures 5(a) and 5(b) elucidate the evolution of EB shift and the change in coercive field under various cooling field strengths. As shown in Fig. 5(a), H_{EB} displays a saturation tendency towards the higher cooling fields, a characteristic usually observed for the archetypal coupled FM and AFM layers [43]. Further, the coercive field H_C is enhanced with increasing cooling fields [Fig. 5(b)] and this signifies the existence of magnetic anisotropy related to pinned spins across the interface of CuO/LSMO bilayer [44,45]. It is to be noted that the observation of exchange bias is not limited to only coupled FM/AFM interfaces. Rather, there have been examples of FM/spin glass (SG) interfaces that also exhibit EB effect [46–48]. To examine the possibility for any coupled FM/spin glass (SG) like interface arising from interfacial spin disorder, we performed thermoremanent magnetization (TRM) measurement. The CuO/LSMO bilayer was cooled down from a temperature $T = 370$ K to measuring temperature (T_M) 2 K under 5 kOe applied field. When the T_M was reached, the applied field was kept for 300 seconds and then the field was removed and the magnetization was measured as a function of time. If the observed EB was due to FM/SG interface, it would be natural to expect time-dependent slow dynamics response in magnetization since SG states possess numerous metastable states. In a SG system, time decay of the TRM generally follows a logarithmic trend [49]. As shown in the inset of Fig. 5(c), the TRM for (CuO/LSMO) bilayer in contrast remains almost constant over four thousand seconds of observation time. Thus, we rule out the possibility of any coupled FM/SG interface resulting in EB effect in CuO/LSMO bilayer.

Further to track the evolution of EB shift with temperature, we measured $M(H)$ loops in FC mode at different temperatures. For each measurement at a fixed temperature, the sample was field cooled from 370 K with an applied field of -1 T and then the hysteresis was measured at the corresponding fixed temperature. To demonstrate the EB effect more clearly, we have adapted inversion method to represent the $M(H)$ loops measured in FC mode [26,43]. In such representation, M and H of the reversing part of the original loop are multiplied by -1 such that the H_{C-} of the original loop shifts to the positive field side. This method of representataion allows to distinguish easily the difference between the H_{C+} of the original loop and H_{C-} of the inverted loop. Enlarged curves of original and inverted hysteresis loops are shown in Fig. 6. It is seen that with increasing temperature, EB effect gradually decreases and vanishes at 5 K.

The variation of H_{EB} and H_C of the CuO/LSMO bilayer as a function of temperature [Figs. 5(c), 5(d), and 6] suggest the disappearance of the EB effect at 5 K. There could be two possible reasons for this observation, (i) the interfacial coupling is too weak, (ii) the associated antiferromagnetic Neel temperature of ultrathin CuO is less than 5 K. Though direct visualization of the spin structure at the interface is a hard nut to crack, few remarks can be made based on the work by Hernández *et al.* in which the authors used low-energy muon spin rotation and x-ray magnetic circular dichroism (XMCD) to investigate the magnetic structure in ultrathin T-CuO thin films [23]. They reported that ultrathin T-CuO has
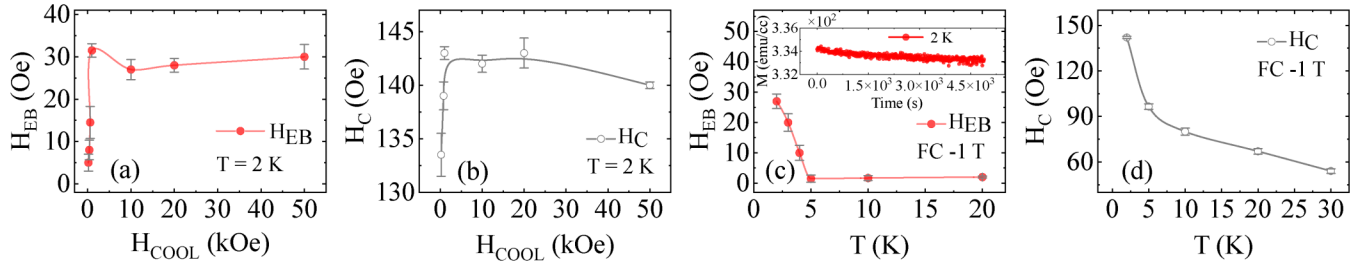
FIG. 5. Exchange shift and change in coercivity of CuO/LSMO sample from EB measurements. [(a) and (b)] Cooling field dependence of H_{EB} and H_C field measured at 2 K. [(c) and (d)] Temperature dependence of H_{EB} and H_C field measured in presence of -1 T magnetic field in FC mode. The inset shows thermoremanent magnetization measured at 2 K. The solid lines are guide to the eyes.

mainly two distinct kind of spin structures, one corresponds to antiferromagnetic moments within the film and the other corresponds to pinned moments close to the surface of the film. They found that the Cu^{2+} moments close to the surface in ultrathin T-CuO get pinned by the antiferromagnetic ordering of the underlying spins in the film plane and it so happens that there is a significant increase in pinning of spins below 3 K. Considering this as a possible model for spin structure arrangement, it is expected that the pinned spin moments of T-CuO layer can couple to spins of LSMO layer strengthening the unidirectional anisotropy by means of interfacial exchange coupling between Mn^{3+}/Mn^{4+} and Cu^{2+} spins below 3 K. However, as the temperature increases, the pinned Cu moments at the interface become gradually reversible and rotate in the direction of field and thus does not provide any substantial unidirectional biasing field on the ferromagnetic LSMO layer to observe the exchange bias. We hypothesize at 5 K Zeeman energy overcomes the interfacial coupling providing a vanishing EB field. Concerning the dimensional effect, it is known that the magnetic transition in ultrathin films can be reduced due to finite size ($[T_m(\infty) - T_m(t)]/T_m(\infty) = (c/t)^\lambda$, where $T_m(\infty)$ is the magnetic transition in the bulk limit, T_m is the magnetic transition temperature of the films with

thickness t, c is related to spin correlation length, and λ is the critical shift exponent) and strain effects [34–36]. However, our earlier study using resonant inelastic x-ray scattering (RIXS) performed at 20 K on ultrathin T-CuO thin films revealed antiferromagnetic spin-wave excitation [22]. Further, the work by Hernández *et al.* based on muon spin polarization decay indicated an AFM order with a transition temperature higher than 200 K. Therefore we rule out the possibility having magnetic order below 5 K for ultrathin T-CuO layer. We conjecture that the observed EB effect is attributed to the weak interfacial exchange coupling between the FM-LSMO and AFM ultrathin T-CuO layers.

C. Ferromagnetic resonance

Figure 7 shows in-plane FMR spectra recorded at various frequencies over the range of 2–12 GHz for the reference bare LSMO (10 nm), CuO ($\sim$1 nm)/LSMO ($\sim$10 nm) bilayer, and LSMO (20 nm) samples. We fit the FMR absorption spectra using the first derivative of Lorentzian symmetric and antisymmetric components described by the equation [50,51]

$$\frac{dP}{dH} = \frac{8C_1 \Delta H (H - H_r)}{[4(H - H_r)^2 + (\Delta H)^2]^2} + \frac{2C_2[(\Delta H)^2 - 4(H - H_r)^2]}{[4(H - H_r)^2 + (\Delta H)^2]^2}, \quad (1)$$

where H is the applied dc field, H_r is the resonance field, ΔH is the full width at the half maximum, and C_1 and C_2 are the amplitudes of the symmetric and antisymmetric Lorentzian derivatives, respectively. Figures 8(a)–8(c) represents H_r as a function of frequency for the bare LSMO (10 nm), CuO/LSMO bilayer, and thick LSMO (20 nm) films using blue, red, and green solid circles, respectively.

The Kittel equation that describes the frequency-dependent resonance field H_r for in-plane configuration is given as [52]

$$f = \frac{\gamma}{2\pi} \sqrt{H_r(H_r + 4\pi M_{\text{eff}})}, \quad (2)$$

where $\gamma = g\mu_B/\hbar$ is the gyromagnetic ratio, and $4\pi M_{\text{eff}} = 4\pi M_S - H_{\text{ani}}$ is the effective saturation induction developed by the magnetic contribution of saturation magnetization $4\pi M_S$ and anisotropy field H_{ani}. The saturation magnetization M_S is calculated from the in-plane measured $M(H)$ loops at 300 K ($M_S \approx 185$, 180, and 210 emu/cc for the bare LSMO (10 nm), CuO/LSMO bilayer, and bare LSMO (20 nm) films, respectively). The extracted values of $4\pi M_{\text{eff}}$ from the fittings
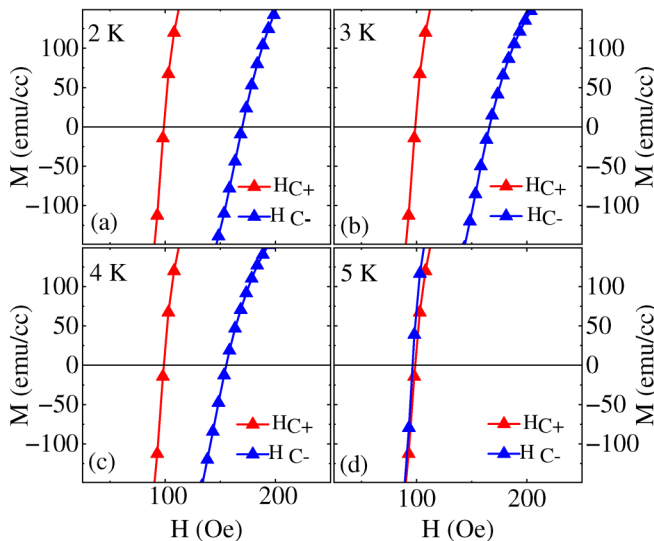

FIG. 6. Magnified view of original and inverted loops of CuO/LSMO bilayer measured at (a) 2, (b) 3, (c) 4, and (d) 5 K, after the FC process.
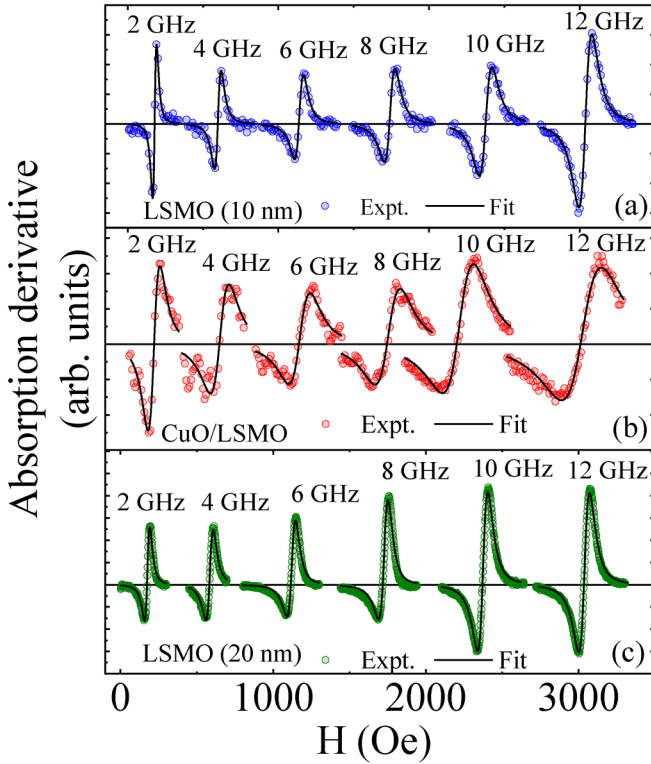
FIG. 7. Room temperature ferromagnetic resonance measurements. FMR derivative spectra measured at different frequencies for 10-nm-thick LSMO (a) without and (b) with 1-nm ultrathin T-CuO interfacial layer, and (c) a 20-nm-thick LSMO samples. The corresponding Lorentzian fits are shown by solid lines for all the samples.
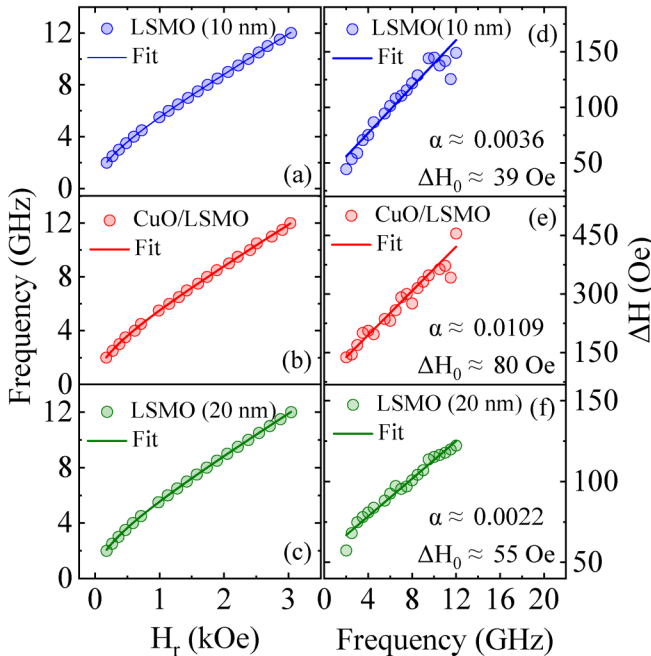

FIG. 8. Frequency-dependent resonance field H_r for (a) LSMO (10 nm), (b) CuO/LSMO bilayer, and (c) LSMO (20 nm) films fitted to the lines shown by solid circles. FMR linewidths as a function of frequency (d) 10-nm LSMO, (e) CuO/LSMO bilayer, and (f) 20-nm LSMO samples.

for the bare LSMO (10 nm), CuO/LSMO bilayer, and thick LSMO (20 nm) films are $\approx$ 2513, 2611, and 2740 Oe, respectively and the corresponding H_{ani} values are -190, -351, and -102 Oe. The frequency-dependent FMR linewidth ΔH for the bare LSMO (10 nm), CuO/LSMO bilayer, and bare LSMO (20 nm) films is depicted in Figs. 8(d)–8(f). The data show a linear fit to the Landau-Lifshitz-Gilbert (LLG) equation expressed as [52,53]

$$\Delta H = \Delta H_0 + \frac{4\pi\alpha}{\sqrt{3}\gamma}f, \qquad (3)$$

where ΔH_0 denotes the inhomogeneous linewidth broadening, usually considered to be an extrinsic inhomogeneous contribution to the linewidth, and α is the Gilbert damping parameter, which generally quantifies the damping contribution to the overall magnetic relaxation processes. Both α and ΔH_0 can be determined from the slopes and zero frequency intercepts on the vertical axis of the linear frequency data, respectively. The (α, ΔH_0) values from the linear fit for the bare LSMO and CuO/LSMO bilayer comes out to be (3.6×10^{-3}, 39 Oe) and (1.09×10^{-2}, 80 Oe), respectively. We observe an enhancement in the slope of the frequency versus linewidth plot for the CuO/LSMO bilayer compared to the bare LSMO (10 nm) layer, which suggests increased precessional damping in the former. The damping enhances by more than three times in the CuO/LSMO bilayer compared to the bare LSMO film. The damping parameter of LSMO (10 nm) film is comparable to the previous reported values [54,55]. Similarly, the α and ΔH_0 values obtained for reference LSMO (20 nm) layer are 2.23×10^{-3} and 55 Oe, respectively.

The contributions leading to the enhancement of magnetic damping can be attributed to two sources, intrinsic damping mechanism (Gilbert type) and spin pumping effect. The intrinsic mechanism responsible for magnetic damping involves breathing Fermi surface model (intraband transition) and the spin-orbit coupling (SOC) mediated s-d exchange interaction (inter-band transition) [56]. However, such a mechanism in weakly spin-orbit coupled systems (LSMO and CuO/LSMO thin films) is unlikely to promote damping via the inter-band transition. This prompts us to explore the role of breathing Fermi surface (BFS) model in which α is directly related to the density of states (DOS) at the Fermi energy [57,58]. From earlier studies, it is evident that the strain affects the minority spin DOS of LSMO at the Fermi energy [59]. The estimated damping parameter of 20-nm LSMO film ($\alpha = 2.23\times10^{-3}$) is less than that of 10-nm LSMO film ($\alpha = 3.6\times10^{-3}$). This discrepancy in damping is believed to stem from thickness effect where the electron-electron scattering at surface might be more pronounced in 10-nm LSMO film compared to the 20-nm LSMO film [59]. However, since both LSMO (10 nm) and CuO ($\sim$1 nm)/LSMO ($\sim$10 nm) are subjected to similar strain effect, the intrinsic mechanism thus cannot be the only factor giving rise to the observed enhancement of the damping value in the bilayer. The FMR line broadens when T-CuO layer is coupled with LSMO layer as compared to LSMO single layer [Figs. 7(a) and 7(b)]. This broadening of linewidth can be attributed to the additional channels of magnetization relaxation stemming from the leakage of magnetization across the CuO/LSMO interface driven by the spin current,

also called spin pumping effect [60]. Considering the above experimental evidence, we invoke a possible scenario where the spin pumping from FM metallic LSMO into T-CuO can be considered as an additional source responsible for the greater damping. Since the spin pumping is inversely proportional to the thickness of the ferromagnetic layer, it is evident that the small thickness of LSMO is more susceptible to showing spin-pumping-induced enhancement in damping [61,62]. The spin transport from LSMO to T-CuO layer leading to the damping can be discussed in terms of the interfacial spin mixing conductance [61],

$$g_{\text{eff}}^{\uparrow\downarrow} = \frac{4\pi M_S t_{\text{LSMO}}}{g\mu_B}(\alpha_{\text{CuO/LSMO}} - \alpha_{\text{LSMO}}), \qquad (4)$$

where t_{LSMO}, g, and μ_B are the thickness of the LSMO film, the Lande g factor, and the Bohr magneton, respectively. For 10-nm LSMO thin film, we calculate, $g_{\text{eff}}^{\uparrow\downarrow} \approx (0.88 \pm 0.034) \times 10^{15}$ cm^{-2}. This value could be compared with $g_{\text{eff}}^{\uparrow\downarrow}$ for interfaces Pt/LSMO $(0.55 \times 10^{15}$ cm$^{-2})$ [63], SrIrO$_3$/LSMO $(0.12 \times 10^{15}$ cm$^{-2})$ [64], SrRuO$_3$/LSMO $(0.5 \times 10^{15}$ cm$^{-2})$ [65], and LSMO/Pt $(0.42 \times 10^{15}$ cm$^{-2})$ [54].

Here, the spin current is generated by the spin pumping effect can occur via the interfacial exchange coupling. The work by Wang *et al.* reports the injection of a spin current into antiferromagnetic NiO from a ferrimagnetic Y$_3$Fe$_5$O$_{12}$ (YIG) by spin pumping through the interfacial exchange coupling [66]. Their finding demonstrates that the magnetic excitations generated in the adjacent insulating NiO layer occur due to the exchange coupling between the precessing YIG magnetization and the spins in NiO across the YIG/NiO interface. This ultimately leads to the broadening of ΔH and an increase in the precessional damping of YIG [66]. Further, Qiu *et al.* probed the temperature dependent spin pumping by employing inverse spin Hall measurement (ISHE) in YIG/CoO/Pt device and detected an enhanced spin pumping effect in the vicinity of Néel temperature of CoO [67]. Moreover, Li *et al.* found that there exists strong enhancement in magnetic damping in YIG/Co$_2$FeAl$_{0.5}$Si$_{0.5}$ bilayer attributed to the interfacial exchange coupling and spin pumping effect at the heterointerface [68]. Based on the above experimental results, we conjecture that the underlying antiferromagnetic spin correlation within the T-CuO layer could drive the spin current by introducing an additional damping in LSMO due to the exchange coupling between LSMO and T-CuO layer. Recently, positive exchange bias due to AFM coupling between LSMO and growth induced interfacial layer has been discussed [69].

A large inhomogeneous $4\pi M_{\text{eff}}$ value was realized, as a direct consequence of AFM exchange coupling at the interface of LSMO and growth-induced interfacial layer [69]. Similarly, Kumar *et al.* report positive exchange bias effect along with enhanced Gilbert damping, FMR linewidth broadening, and large inhomogeneous $4\pi M_{\text{eff}}$ because of AFM exchange coupling at the interface of YIG and the growth-induced interfacial layer [52]. If we compare the $4\pi M_{\text{eff}}$ values of the bare 10-nm-thick LSMO ($\sim$2513 Oe) and CuO/LSMO ($\sim$2611 Oe) samples, the value is larger in the latter, corroborating with the above findings. Thus, from the above discussion, we emphasize that LSMO couples antiferromagnetically with the ultrathin T-CuO layer leading to interfacial exchange bias effect.

IV. CONCLUSION

In summary, we successfully synthesized tetragonal-CuO/LSMO interface and uncovered a positive exchange bias effect at low temperature, cofirming the antiferromagnetic ordering in ultrathin T-CuO layer. Because of the ultrathin limit of T-CuO ($\sim$1 nm) layer, the interfacial pinning effect appeared to be weak, thus causing the EB effect to vanish above 5 K. Furthermore, we leveraged the FMR technique at 300 K to investigate the exchange interaction at the interface between LSMO and the T-CuO layer. We noted a threefold increase in the Gilbert damping parameter in the CuO/LSMO bilayer compared to the standalone LSMO layer (10 nm), suggesting the presence of interfacial exchange coupling. Moreover, this interlayer exchange coupling allows envisaging the possible spin mixing conductance at the CuO/LSMO heterointerface leading to an enhancement in damping. Additionally, our observations included a higher inhomogeneous value of effective magnetization in the CuO/LSMO bilayer, further supporting the presence of interfacial exchange coupling. Our findings based on static and magnetization study suggests the possibility of underlying AFM correlations, be they static or fluctuating, within T-CuO layer.

ACKNOWLEDGMENTS

---

[1] J. G. Bednorz and K. A. Mueller, Possible high Tc superconductivity in the Ba-La-Cu-O system, Z. Phys. B **64**, 189 (1986).

[2] B. Keimer, S. Kivelson, M. Norman, S. Uchida, and J. Zaanen, From quantum matter to high-temperature superconductivity in copper oxides, Nature (London) **518**, 179 (2015).

[3] P. A. Lee, N. Nagaosa, and X.-G. Wen, Doping a mott insulator: Physics of high-temperature superconductivity, Rev. Mod. Phys. **78**, 17 (2006).

[4] S. Åsbrink and L.-J. Norrby, A refinement of the crystal structure of copper (II) oxide with a discussion of some exceptional esd's, Acta Cryst. Sect. B **26**, 8 (1970).

[5] H. Jacobsen, S. M. Gaw, A. J. Princep, E. Hamilton, S. Tóth, R. A. Ewings, M. Enderle, E. M. H. Wheeler, D. Prabhakaran, and A. T. Boothroyd, Spin dynamics and exchange interactions in CuO measured by neutron scattering, Phys. Rev. B **97**, 144401 (2018).

[6] S. H. Jung, J. Kim, E. J. Choi, Y. Sekio, T. Kimura, and J. Lorenzana, Infrared optical absorption spectra of CuO single crystals: Fermion-spinon band and dimensional crossover of the antiferromagnetic order, Phys. Rev. B **80**, 140516(R) (2009).

[7] A. Boothroyd, A. Mukherjee, S. Fulton, T. Perring, R. Eccleston, H. Mook, and B. Wanklyn, High-energy magnetic

excitations in CuO, Phys. B: Condens. Matter **234-236**, 731 (1997).

[8] T. Kimura, Y. Sekio, H. Nakamura, T. Siegrist, and A. Ramirez, Cupric oxide as an induced-multiferroic with high-T_C, Nat. Mater. **7**, 291 (2008).

[9] A. Filippetti and V. Fiorentini, Magnetic ordering in CuO from first principles: a cuprate antiferromagnet with fully three-dimensional exchange interactions, Phys. Rev. Lett. **95**, 086405 (2005).

[10] L. F. Mattheiss, Electronic structure of the $3d$ transition-metal monoxides. I. energy-band results, Phys. Rev. B **5**, 290 (1972).

[11] K. Terakura, T. Oguchi, A. R. Williams, and J. Kübler, Band theory of insulating transition-metal monoxides: Band-structure calculations, Phys. Rev. B **30**, 4734 (1984).

[12] W. A. Harrison, Heisenberg exchange in the magnetic monoxides, Phys. Rev. B **76**, 054417 (2007).

[13] G. Fischer, M. Däne, A. Ernst, P. Bruno, M. Lüders, Z. Szotek, W. Temmerman, and W. Hergert, Exchange coupling in transition metal monoxides: Electronic structure calculations, Phys. Rev. B **80**, 014408 (2009).

[14] B. X. Yang, T. R. Thurston, J. M. Tranquada, and G. Shirane, Magnetic neutron scattering study of single-crystal cupric oxide, Phys. Rev. B **39**, 4343 (1989).

[15] W. Siemons, G. Koster, D. H. A. Blank, R. H. Hammond, T. H. Geballe, and M. R. Beasley, Tetragonal CuO: End member of the $3d$ transition metal monoxides, Phys. Rev. B **79**, 195122 (2009).

[16] D. Samal, H. Tan, Y. Takamura, W. Siemons, J. Verbeeck, G. Van Tendeloo, E. Arenholz, C. Jenkins, G. Rijnders, and G. Koster, Direct structural and spectroscopic investigation of ultrathin films of tetragonal CuO: Six-fold coordinated copper, Europhys. Lett. **105**, 17003 (2014).

[17] S. Moser, L. Moreschini, H.-Y. Yang, D. Innocenti, F. Fuchs, N. H. Hansen, Y. J. Chang, K. S. Kim, A. L. Walter, A. Bostwick, E. Rotenberg, F. Mila, and M. Grioni, Angle-resolved photoemission spectroscopy of tetragonal CuO: Evidence for intralayer coupling between cupratelike sublattices, Phys. Rev. Lett. **113**, 187001 (2014).

[18] I. J. Hamad, L. O. Manuel, and A. A. Aligia, Generalized one-band model based on Zhang-Rice singlets for tetragonal CuO, Phys. Rev. Lett. **120**, 177001 (2018).

[19] Y. Zhong, Z. Dou, R.-F. Wang, Y.-F. Lv, S. Han, H. Yan, C.-L. Song, X.-C. Ma, and Q.-K. Xue, Real-space characterization of tetragonal CuO epitaxial films, Appl. Phys. Lett. **119**, 172602 (2021).

[20] X.-Q. Chen, C. L. Fu, C. Franchini, and R. Podloucky, Hybrid density-functional calculation of the electronic and magnetic structures of tetragonal CuO, Phys. Rev. B **80**, 094527 (2009).

[21] G. Peralta, D. Puggioni, A. Filippetti, and V. Fiorentini, Jahn-Teller stabilization of magnetic and orbital ordering in rocksalt CuO, Phys. Rev. B **80**, 140408(R) (2009).

[22] S. Moser, N. E. Shaik, D. Samal, S. Fatale, B. Dalla Piazza, M. Dantz, J. Pelliciari, P. Olalde-Velasco, T. Schmitt, G. Koster, F. Mila, H. M. Rønnow, and M. Grioni, Magnons in tetragonal CuO, Phys. Rev. B **92**, 140404(R) (2015).

[23] N. Ortiz Hernández, Z. Salman, T. Prokscha, A. Suter, J. R. L. Mardegan, S. Moser, A. Zakharova, C. Piamonteze, and U. Staub, Magnetic order of tetragonal CuO ultrathin films, Phys. Rev. B **103**, 224429 (2021).

[24] J. Nogués and I. K. Schuller, Exchange bias, J. Magn. Magn. Mater. **192**, 203 (1999).

[25] A. Berkowitz and K. Takano, Exchange anisotropy - a review, J. Magn. Magn. Mater. **200**, 552 (1999).

[26] Y. Zhou, L. Miao, P. Wang, F. F. Zhu, W. X. Jiang, S. W. Jiang, Y. Zhang, B. Lei, X. H. Chen, H. F. Ding, H. Zheng, W. T. Zhang, J.-f. Jia, D. Qian, and D. Wu, Antiferromagnetic order in epitaxial FeSe films on $SrTiO_3$, Phys. Rev. Lett. **120**, 097001 (2018).

[27] J. Nogues, D. Lederman, T. Moran, and I. K. Schuller, Positive exchange bias in FeF_2-Fe bilayers, Phys. Rev. Lett. **76**, 4624 (1996).

[28] T. Hong, Simple mechanism for a positive exchange bias, Phys. Rev. B **58**, 97 (1998).

[29] T. Hahn, U. Shmueli, and J. W. Arthur, *International Tables for Crystallography*, Vol. 1 (Reidel, Dordrecht, 1983).

[30] P. Radaelli, G. Iannone, M. Marezio, H. Hwang, S. Cheong, J. Jorgensen, and D. Argyriou, Structural effects on the magnetic and transport properties of perovskite $A_{1-x}A'_x MnO_3$ ($x = 0.25$, 0.30), Phys. Rev. B **56**, 8265 (1997).

[31] B. Cui, C. Song, F. Li, X. Y. Zhong, Z. C. Wang, P. Werner, Y. D. Gu, H. Q. Wu, M. S. Saleem, S. S. P. Parkin, and F. Pan, Electric-field control of oxygen vacancies and magnetic phase transition in a cobaltite/manganite bilayer, Phys. Rev. Appl. **8**, 044007 (2017).

[32] X. Zheng, S. Channa, L. Riddiford, J. Wisser, K. Mahalingam, C. Bowers, M. McConney, A. N'Diaye, A. Vailionis, E. Cogulu, H. Ren, Z. Galazka, A. Kent, and Y. Suzuki, Ultra-thin lithium aluminate spinel ferrite films with perpendicular magnetic anisotropy and low damping, Nat. Commun. **14**, 4918 (2023).

[33] Y. Lee, S. Park, Y. Hyun, J. Kim, V. Prokhorov, V. Komashko, and V. Svetchnikov, Microstructural and magnetotransport properties of $La_{0.7}Ca_{0.3}MnO_3/BaTiO_3$ and $La_{0.7}Sr_{0.3}MnO_3/BaTiO_3$ bilayered films, Phys. Rev. B **73**, 224413 (2006).

[34] F. Yang, N. Kemik, M. D. Biegalski, H. M. Christen, E. Arenholz, and Y. Takamura, Strain engineering to control the magnetic and magnetotransport properties of $La_{0.67}Sr_{0.33}MnO_3$ thin films, Appl. Phys. Lett. **97**, 092503 (2010).

[35] L. Yin, C. Wang, Q. Shen, and L. Zhang, Strain-induced Curie temperature variation in $La_{0.9}Sr_{0.1}MnO_3$ thin films, RSC Adv. **6**, 96093 (2016).

[36] M. E. Fisher and M. N. Barber, Scaling theory for finite-size effects in the critical region, Phys. Rev. Lett. **28**, 1516 (1972).

[37] B. Kim, D. Kwon, J. H. Song, Y. Hikita, B. G. Kim, and H. Y. Hwang, Finite size effect and phase diagram of ultra-thin $La_{0.7}Sr_{0.3}MnO_3$, Solid State Commun. **150**, 598 (2010).

[38] H. C. Siegmann and J. Stöhr, *Magnetism: From Fundamentals to Nanoscale Dynamics* (Springer, Berlin, 2006).

[39] R. Palai, H. Huhtinen, J. Scott, and R. Katiyar, Observation of spin-glass-like behavior in $SrRuO_3$ epitaxial thin films, Phys. Rev. B **79**, 104413 (2009).

[40] C.-C. Liu, P.-Y. Chu, Y.-W. Chiang, J.-Y. Juang, and S.-U. Jen, Magnetic domain studies of $La_{0.7}Sr_{0.3}MnO_3$ film deposited on $SrLaAlO_4$ (0 0 1) substrate, J. Phys. D **46**, 255001 (2013).

[41] W. H. Meiklejohn and C. P. Bean, New magnetic anisotropy, Phys. Rev. **102**, 1413 (1956).

[42] W. H. Meiklejohn and C. P. Bean, New magnetic anisotropy, Phys. Rev. **105**, 904 (1957).

[43] B. Behera, S. Jana, S. G. Bhat, N. Gauquelin, G. Tripathy, P. A. Kumar, and D. Samal, Evidence for exchange bias coupling at the perovskite/brownmillerite interface in spontaneously stabilized $SrCoO_{3-\delta}$/$SrCoO_{2.5}$ bilayers, Phys. Rev. B **99**, 024425 (2019).

[44] X. Ning, Z. Wang, X. Zhao, C. Shih, and Z. Zhang, Exchange bias in $La_{0.7}Sr_{0.3}MnO_3$/NiO and $LaMnO_3$/NiO interfaces, J. Appl. Phys. **113**, 223903 (2013).

[45] Y. Tian, O. Lebedev, V. Roddatis, W. Lin, J. Ding, S. Hu, S. Yan, and T. Wu, Interfacial magnetic coupling in ultrathin all-manganite $La_{0.7}Sr_{0.3}MnO_3 - TbMnO_3$ superlattices, Appl. Phys. Lett. **104**, 152404 (2014).

[46] M. Gibert, P. Zubko, R. Scherwitzl, J. Íñiguez, and J.-M. Triscone, Exchange bias in $LaNiO_3 - LaMnO_3$ superlattices, Nat. Mater. **11**, 195 (2012).

[47] M. Ali, P. Adie, C. H. Marrows, D. Greig, B. J. Hickey, and R. L. Stamps, Exchange bias using a spin glass, Nat. Mater. **6**, 70 (2007).

[48] G. Salazar-Alvarez, J. Sort, S. Surinach, M. D. Baró, and J. Nogués, Synthesis and size-dependent exchange bias in inverted core- shell $MnO|Mn_3O_4$ nanoparticles, J. Am. Chem. Soc. **129**, 9102 (2007).

[49] J. A. Mydosh, *Spin Glasses: An Experimental Introduction* (CRC Press, Cambridge, MA, 1993).

[50] N. Mecking, Y. Gui, and C.-M. Hu, Microwave photovoltage and photoresistance effects in ferromagnetic microstrips, Phys. Rev. B **76**, 224430 (2007).

[51] P. Dürrenfeld, F. Gerhard, J. Chico, R. K. Dumas, M. Ranjbar, A. Bergman, L. Bergqvist, A. Delin, C. Gould, L. W. Molenkamp, and J. Åkerman, Tunable damping, saturation magnetization, and exchange stiffness of half-Heusler NiMnSb thin films, Phys. Rev. B **92**, 214424 (2015).

[52] R. Kumar, B. Samantaray, S. Das, K. Lal, D. Samal, and Z. Hossain, Damping in yttrium iron garnet films with interface, Phys. Rev. B **106**, 054405 (2022).

[53] H. Chang, P. Praveen Janantha, J. Ding, T. Liu, K. Cline, J. N. Gelfand, W. Li, M. C. Marconi, and M. Wu, Role of damping in spin Seebeck effect in yttrium iron garnet thin films, Sci. Adv. **3**, e1601614 (2017).

[54] I. Benguettat-El Mokhtari, Y. Roussigné, T. Petrisor Jr, F. Zighem, F. Kail, L. Chahed, V. Pierron, L. Méchin, M. Gabor, and M. Belmeguenai, Spin pumping and magnetic anisotropy in $La_{2/3}Sr_{1/3}MnO_3$/Pt systems, physica status solidi (b) **257**, 2000265 (2020).

[55] A. Das, Mrinalini, T. Usami, S. Pati, T. Taniyama, and V. Gorige, Electric and magnetic tuning of Gilbert damping constant in LSMO/PMN-PT (011) heterostructure, J. Phys.: Condens. Matter **35**, 285801 (2023).

[56] B. Heinrich, D. Fraitová, and V. Kamberský, The influence of s-d exchange on relaxation of magnons in metals, physica status solidi (b) **23**, 501 (1967).

[57] H. Ebert, S. Mankovsky, D. Ködderitzsch, and P. J. Kelly, Ab Initio calculation of the gilbert damping parameter via the linear response formalism, Phys. Rev. Lett. **107**, 066603 (2011).

[58] S. Lounis, M. dos Santos Dias, and B. Schweflinghaus, Transverse dynamical magnetic susceptibilities from regular static density functional theory: Evaluation of damping and *g* shifts of spin excitations, Phys. Rev. B **91**, 104420 (2015).

[59] Q. Qin, S. He, W. Song, P. Yang, Q. Wu, Y. P. Feng, and J. Chen, Ultra-low magnetic damping of perovskite $La_{0.7}Sr_{0.3}MnO_3$ thin films, Appl. Phys. Lett. **110**, 112401 (2017).

[60] G. Ovsyannikov, T. Shaikhulov, K. Stankevich, Y. Khaydukov, and N. Andreev, Magnetism at an iridate/manganite interface: Influence of strong spin-orbit interaction, Phys. Rev. B **102**, 144401 (2020).

[61] Y. Tserkovnyak, A. Brataas, and G. E. Bauer, Enhanced gilbert damping in thin ferromagnetic films, Phys. Rev. Lett. **88**, 117601 (2002).

[62] Y. Tserkovnyak, A. Brataas, and G. E. Bauer, Spin pumping and magnetization dynamics in metallic multilayers, Phys. Rev. B **66**, 224403 (2002).

[63] H. K. Lee, I. Barsukov, A. Swartz, B. Kim, L. Yang, H. Hwang, and I. Krivorotov, Magnetic anisotropy, damping, and interfacial spin transport in Pt/LSMO bilayers, AIP Adv. **6**, 052212 (2016).

[64] S. Crossley, A. Swartz, K. Nishio, Y. Hikita, and H. Hwang, All-oxide ferromagnetic resonance and spin pumping with $SrIrO_3$, Phys. Rev. B **100**, 115163 (2019).

[65] S. Emori, U. S. Alaan, M. T. Gray, V. Sluka, Y. Chen, A. D. Kent, and Y. Suzuki, Spin transport and dynamics in all-oxide perovskite $La_{2/3}Sr_{1/3}MnO_3$/SrRuO$_3$ bilayers probed by ferromagnetic resonance, Phys. Rev. B **94**, 224423 (2016).

[66] H. Wang, C. Du, P. C. Hammel, and F. Yang, Spin transport in antiferromagnetic insulators mediated by magnetic correlations, Phys. Rev. B **91**, 220410(R) (2015).

[67] Z. Qiu, J. Li, D. Hou, E. Arenholz, A. T. N'Diaye, A. Tan, K.-i. Uchida, K. Sato, S. Okamoto, Y. Tserkovnyak, Z. Q. Qiu, and E. Saitoh, Spin-current probe for phase transition in an insulator, Nat. Commun. **7**, 12670 (2016).

[68] M. Li, H. Zhang, Y. Rao, C. Hong, Z. Zhong, Q. Yang, X. Tang, and L. Jin, Giant damping enhancement induced by exchange coupling in $Y_3Fe_5O_{12}$/$Co_2FeAl_{0.5}Si_{0.5}$ bilayers, J. Alloys Compd. **767**, 398 (2018).

[69] P. Ghising, B. Samantaray, and Z. Hossain, Spin inhomogeneities at the interface and inverted hysteresis loop in $La_{0.7}Sr_{0.3}MnO_3$/SrTiO$_3$, Phys. Rev. B **101**, 024408 (2020).